

# Random matrix perspective on probabilistic error cancellation

Leonhard Moske <sup>1</sup>, Pedro Ribeiro,<sup>2</sup> Tomaž Prosen,<sup>3</sup> Sergiy Denysov,<sup>4</sup> Karol Życzkowski,<sup>5,6</sup> and David J. Luitz <sup>1</sup>

<sup>1</sup>*Institute of Physics, University of Bonn, Nußallee 12, 53115 Bonn*

<sup>2</sup>*CeFEMA-LaPMET, Departamento de Física, Instituto Superior Tecnico, Universidade de Lisboa, Av. Rovisco Pais, 1049-001 Lisboa, Portugal*

<sup>3</sup>*Faculty of Mathematics and Physics, University of Ljubljana, Jadranska 19, SI-1000 Ljubljana, Slovenia*

<sup>4</sup>*Department of Computer Science, OsloMet – Oslo Metropolitan University, Pilestredet 52, Oslo, N-0130, Norway*

<sup>5</sup>*Faculty of Physics, Astronomy and Applied Computer Science, Jagiellonian University, 30-348 Kraków, Poland*

<sup>6</sup>*Center for Theoretical Physics, Polish Academy of Sciences, Al. Lotników 32/46, 02-668 Warszawa, Poland*

Probabilistic error cancellation is an attempt to reverse the effect of dissipative noise channels on quantum computers by applying unphysical channels after the execution of a quantum algorithm on noisy hardware. We investigate on general grounds the properties of such unphysical quantum channels by considering a random matrix ensemble modeling noisy quantum algorithms. We show that the complex spectra of denoiser channels inherit their structure from random Lindbladians. Additional structure imposed by the locality of noise channels of the quantum computer emerges in terms of a hierarchy of timescales.

## I. INTRODUCTION

Current quantum computing hardware is able to execute quantum circuits on a large set of qubits, but the target circuit defined by the quantum algorithm is altered by physical noise channels which prevent the reliable execution of deep circuits required by applications [1, 2]. Circumventing this major obstacle is hence an important issue in the field and is tackled from two angles: Error mitigation [3–10] tries to undo or reduce the effect of the noise while fault tolerant error correction [11–13] introduces redundancy which allows for the correction of errors caused by the noise. It is likely that a combination of both approaches is required for a true breakthrough in the near term.

While dissipative processes are ubiquitous in hardware, their precise nature is unknown and depends on the involved qubits and gates in the circuit. This poses a major challenge for probabilistic error cancellation and extracting the dominant processes is an expensive task, although it can be reduced to a simpler problem by techniques such as Pauli twirling [2, 5].

The standard approach for probabilistic error cancellation inserts an unphysical channel layer at multiple points in the target circuit [5]. In [14] it was proposed to instead use a single operator at the end of the circuit. The upside is that it reduces the number of gates, reducing the required runs of the circuit. This operator, which retrieves the unitary circuit from the noisy quantum channel is called *denoiser*.

Here we start from a general point of view and assume no prior information on the nature of the noise channels and circuits. It is then reasonable to consider an ensemble of circuits, built from unitary operations (modeling the target circuit) and noise channels generated by random Lindbladians to ensure that we get a completely positive trace preserving (CPTP) map. For each noisy sample circuit we can then define a denoiser channel which recovers the target circuit in order to investigate properties of such denoisers on general grounds.

We show that the ensemble of denoisers can effectively be understood in terms of the ensemble of random Lindblad generators [15–19], which feature a universal spectral support. Completely random Lindbladians represent only a crude model of physical dissipation processes. We therefore refine our ensemble by restricting noise to local (few-qubit) processes, where an emergent hierarchy of dissipation timescales was observed [16, 20]. Here we show that this structure reappears in the corresponding denoisers.

## II. MODEL

We introduce a simple model for an ensemble of noisy quantum circuits  $\Lambda_U$  of depth  $m$  acting on  $L$  qubits. We work directly in the folded picture of matrixised superoperators acting on vectorized density matrices. The model has two key ingredients: Unitary operators  $\mathcal{U}_i \in \mathbb{C}^{4^L}$  represent the action of unitary gates of the target quantum algorithm. For simplicity, we construct these matrices as global random unitary matrices, drawn from the Haar measure. One can view a matrix  $\mathcal{U}_i$  as the action of one or multiple layers of a circuit consisting of local gates.

The noise is introduced by noise channels  $\mathcal{N}_i \in \mathbb{C}^{4^L}$  after each layer  $\mathcal{U}_i$  of the circuit, such that the full channel is given by

$$\Lambda_U = \mathcal{N}_m \mathcal{U}_m \dots \mathcal{N}_2 \mathcal{U}_2 \mathcal{N}_1 \mathcal{U}_1. \quad (1)$$

This formulation is similar to the model used in [5], where each unitary circuit layer is paired with a quantum channel to model a noisy quantum device.

The quantum state of the  $L$  qubits is encoded as a density matrix  $\rho$ , which we vectorize as  $|\rho\rangle\rangle$ . The superoperator formalism allows for a direct characterization of the full spectrum of the channel  $\Lambda_U$ . Each pair of  $\mathcal{U}_i$  and  $\mathcal{N}_i$  is understood as one out of a total of  $m$  layers of the noisy circuit.

$$\Lambda_U |\rho\rangle\rangle = \mathcal{N}_m \mathcal{U}_m \dots \mathcal{N}_2 \mathcal{U}_2 \mathcal{N}_1 \mathcal{U}_1 |\rho\rangle\rangle. \quad (2)$$

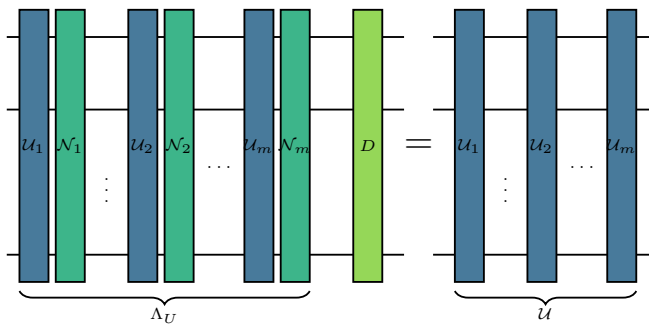


FIG. 1. Diagrammatic representation of eq. (5) defining the denoiser  $D$ . Each layer of the noisy circuit  $\Lambda_U$  consists of a unitary operation  $\mathcal{U}_i$  followed by a noise channel  $\mathcal{N}_i$ . The denoiser  $D$  recovers the target unitary circuit  $\mathcal{U}$  from the noisy channel  $\Lambda_U$ .

We denote the dimension of the Hilbert space of wave functions  $N = 2^L$ . All superoperators then act on the space of dimension  $N^2 = 4^L$ .

For modeling noisy quantum hardware, the regime of *weak* noise is most relevant. We therefore model the noise channels  $\mathcal{N}_i$  using Lindblad generators  $\mathcal{L}_i$  acting for short times  $t \leq 1$ . The noise channels are then given by:

$$\mathcal{N}_i = \exp(t\mathcal{L}_i). \quad (3)$$

The timescale  $t$  allows us to tune the strength of the noise and  $t = 0$  corresponds to the unitary limit in which we have no noise at all.

Modeling the effect of noise by Markovian dynamics appears to be well justified on transmon platforms as confirmed by full process tomography [2, 5].

In the folded picture, the unitary operators are given by the tensor product

$$\mathcal{U}_i = U_i \otimes U_i^T \quad (4)$$

and we sample the factors  $U_i$  i.i.d. as random unitary matrices from the Haar measure, i.e. from  $\text{CUE}(2^L)$ . This means that  $U_i$  is a global operation on the set of qubits and our model features minimal structure.

We define the *denoiser*  $D$  as the operator that recovers the unitary target quantum circuit  $\mathcal{U}$  from  $\Lambda_U$ :

$$D\Lambda_U = \mathcal{U}. \quad (5)$$

Here  $\mathcal{U} = \mathcal{U}_m \dots \mathcal{U}_2 \mathcal{U}_1$  is the combination of the layers without noise, i.e. the target circuit. It can also be recovered by setting the dissipation time to  $t = 0$ . We show a diagram of the equation defining the denoiser in Fig. 1. It is important to note that, since the system undergoes irreversible decoherence due to the environment, the denoiser can not be a completely positive, trace preserving map and is hence an unphysical channel. The denoiser can formally be defined using the inverse of  $\Lambda_U$ :

$$D = \mathcal{U}\Lambda_U^{-1}. \quad (6)$$

This implies that the denoiser can only be defined for invertible channels  $\Lambda_U$ , i.e. if the spectrum of  $\Lambda_U$  lies on the punctured complex plane  $\mathbb{C} \setminus 0$ .

### III. NUMERICAL INVESTIGATION OF THE DENOISER SPECTRA

The Lindbladians [15, 21, 22] are generated using

$$\mathcal{L} = \sum_{l,k=0}^{N^2-2} K_{k,l} \left[ F_l \otimes F_k^* - \frac{1}{2} \left( F_k^\dagger F_l \otimes \mathbb{1} + \mathbb{1} \otimes F_l^T F_k^* \right) \right].$$

The  $F_l$  form an orthogonal basis of the operator space of dimension  $N$ , satisfying  $\text{Tr}(F_l F_k^\dagger) = \delta_{l,k}$ , while also being traceless  $\text{Tr}(F_l) = 0$ . The complex Kossakowski matrix  $K$  carries the information on the coupling to the environment and is positive semi-definite. For purely random Lindblad generators we sample  $K$  from the Wishart ensemble. Concretely it is generated as [23]

$$K = N \frac{G^\dagger G}{\text{Tr}(G^\dagger G)}, \quad (7)$$

where  $G$  is sampled from the square complex Ginibre ensemble, meaning a matrix of order  $N^2 - 1$  with independent Gaussian entries. The normalization of  $K$  is chosen such that the support of the Lindblad spectrum is centered at  $-1$ . In [15] it was shown that the shape of the spectra follows an universal behavior, independent of the sampling of  $K$ .

In order to be able to sample random Lindbladians efficiently we diagonalize the Kossakowski matrix  $K = Q^\dagger D Q$  to reduce the number of terms in the Lindblad generators. The diagonalized equation reads

$$\mathcal{L}_D = \sum_{\mu=0}^{N^2-2} D_{\mu,\mu} \left[ F_\mu \otimes F_\mu^* - \frac{1}{2} \left( F_\mu^\dagger F_\mu \otimes \mathbb{1} + \mathbb{1} \otimes F_\mu^T F_\mu^* \right) \right].$$

With  $F_\mu = \sum_{n=0}^{N^2-2} Q_{\mu,n} F_n$ . The spectra of the ensemble of Lindblad generators can be found in appendix A, Fig. 9.

The  $U_i$  are uniform random unitary matrices with respect to the Haar measure. This is done by populating a matrix  $H$  with random complex numbers sampled from a standard normal distribution, performing a QR decomposition  $H = QR$ , and then taking the matrix  $Q$  as a sample for  $U_i$ , discussed in [24, 25].

The denoiser is then directly calculated as

$$D = \mathcal{U}\Lambda_U^{-1}. \quad (8)$$

The spectra of chosen noisy circuits and the corresponding denoisers are shown in Fig. 2. Since for  $m = 1$  the denoiser only corresponds to an inverse of  $\mathcal{N}_1$ , we set the number of circuit layers to  $m \geq 2$ .

We see that the spectra of the noisy circuit for small  $t$  is close to the unit circle. This is expected as for  $t$  going to 0 the noisy circuit is approaching the unitary case. The denoiser eigenvalues have modulus greater than 1, highlighting the fact that the denoiser is an unphysical

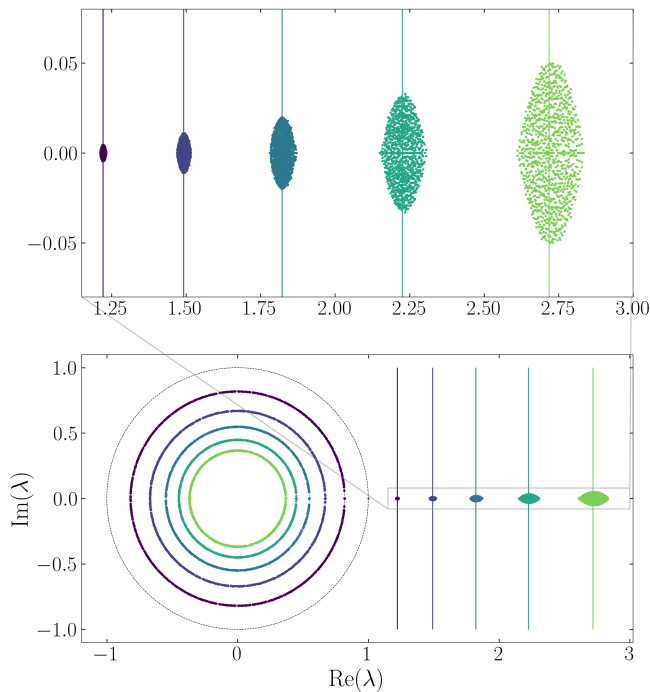


FIG. 2. Spectra of  $\Lambda_U$  and the denoiser  $D$  for different noise parameters  $t = [0.1, 0.2, 0.3, 0.4, 0.5]$ , with  $N = 32$  and  $m = 2$ . The spectra of the noisy channel lie inside the unit circle, while the denoiser spectra lie outside, centered around the real axis. For small noise  $t$  the spectrum of the noisy channel is close to the unit circle, while the denoiser is close to the identity with eigenvalue 1. With increasing  $t$  the noisy channel spectrum moves towards the center of the unit circle, while the denoiser spectrum increases in modulus and moves away from 1. We draw the predicted centers of the denoiser for different  $t$  as vertical lines at  $\exp(mt)$ , according to Eq. (17).

operator. As a consequence of quantum channels being completely positive (i.e. preserving Hermiticity) the eigenvalues of  $\Lambda_U$  come in conjugate pairs [26]. With  $t$  increasing, the eigenvalues of the noisy circuit decrease in modulus, which implies increasing decay rates with only the steady state at 1 surviving in the  $t \rightarrow \infty$  case. In consequence the eigenvalues of the denoiser increase in modulus with growing  $t$ .

The denoiser spectra for different system sizes  $N$  is shown in Fig. 3. For larger system sizes the support of the spectrum condenses. This is a result of the behavior of the Lindblad spectrum, which also condenses around  $-1$  with extent  $2/N$  as shown in [15].

In Fig. 4 we show the denoiser spectra for different number of layers  $m$ . For larger  $m$  the denoiser eigenvalues increase in modulus and the support of the spectrum expands. We will explain this behavior in the next section. Intuitively, more layers of noise need to be inverted by the denoiser, which leads to larger eigenvalues.

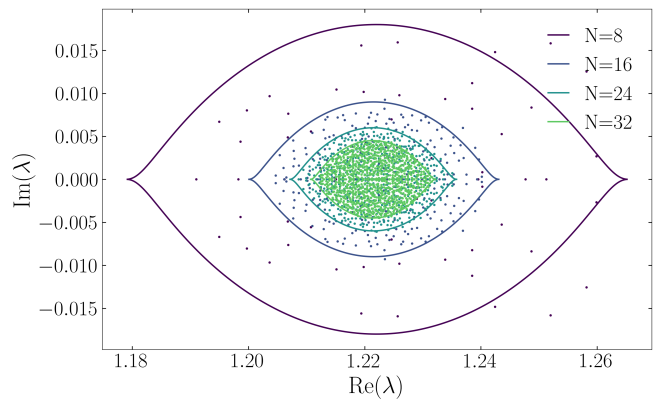


FIG. 3. denoiser spectra for different system sizes  $N = [8, 16, 24, 32]$ . Here  $t = 0.1$  and  $m = 2$ . For readability we exclude the stationary point at 1 and we include the prediction of the contour discussed in the next section.

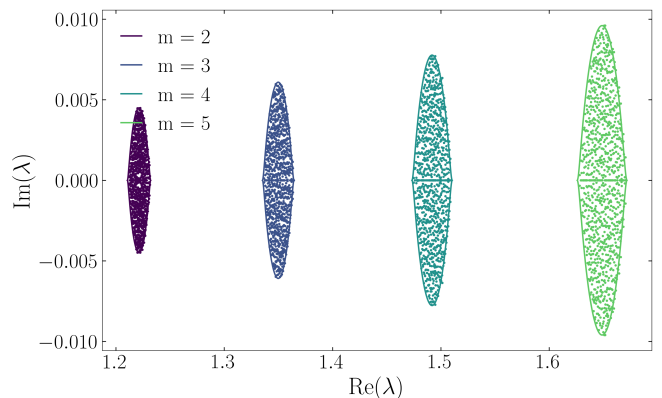


FIG. 4. denoiser spectra for different  $m = [2, 3, 4, 5]$ . Here  $t = 0.1$  and  $N = 32$ . For readability we exclude the stationary point at 1 and we include the prediction of the contour discussed in the next section.

#### IV. REFORMULATION OF DENOISER USING THE BAKER-CAMPBELL-HAUSDORFF FORMULA

In the previous section we observed different behaviors of the spectral support of the denoiser with respect to the parameters of the model  $N, t$  and  $m$ . To understand the different behaviors we want to reformulate the noisy channel.

First we recognize that we can change the order of  $\mathcal{U}_i$  and  $\mathcal{N}_i$  in layer  $i$  by using the fact that  $\mathcal{U}_i$  is a unitary operator.

$$\mathcal{U}_j \exp(t\mathcal{L}_i) = \mathcal{U}_j \exp(t\mathcal{L}_i) \mathcal{U}_j^\dagger \mathcal{U}_j \quad (9)$$

$$= \exp(t\mathcal{U}_j \mathcal{L}_i \mathcal{U}_j^\dagger) \mathcal{U}_j \quad (10)$$

$$= \exp(t\tilde{\mathcal{L}}_i) \mathcal{U}_j. \quad (11)$$

The only difference is that the Lindbladian is trans-

formed by the unitary, but since the unitary is sampled from the Haar measure, the ensemble of  $\mathcal{L}$  and  $\tilde{\mathcal{L}}_i$  is the same. This means that we can rewrite the noisy circuit as

$$\Lambda_U = \dots \exp(t\mathcal{L}_2)\mathcal{U}_2 \exp(t\mathcal{L}_1)\mathcal{U}_1 \quad (12)$$

$$= \left[ \prod_i^m \exp(t\tilde{\mathcal{L}}_i) \right] \mathcal{U}. \quad (13)$$

The rotated Lindbladians are given by  $\tilde{\mathcal{L}}_i := \left( \prod_{j=0}^{i-1} \mathcal{U}_{m-j} \right) \mathcal{L}_i \left( \prod_{j=i+1}^m \mathcal{U}_j^\dagger \right)$ . From equation 5 we can identify the inverse of the denoiser as

$$D^{-1} = \left[ \prod_i^m \exp(t\tilde{\mathcal{L}}_i) \right]. \quad (14)$$

Using the Baker-Campbell-Hausdorff (BCH) formula we can combine the exponentials to

$$D^{-1} = \exp \left( t \left( \sum_i^m \tilde{\mathcal{L}}_i \right) + \frac{t^2}{2} \left( \sum_{j<k} [\tilde{\mathcal{L}}_j, \tilde{\mathcal{L}}_k] \right) + \mathcal{O}(t^3) \right),$$

where the higher order terms include higher order commutators of the Lindblad generators. We assume that the noise scale  $t$  is small, and approximate the denoiser only with linear terms in  $t$ ,

$$D^{-1} = \exp \left( t \sum_i^m \tilde{\mathcal{L}}_i \right). \quad (15)$$

The operator can be inverted by negating the exponent to retrieve an approximation of  $D$ .

In appendix, B Fig. 11 we show the comparison of the exact denoiser spectra and approximations by the linear term, for different combinations of  $t$  and  $m$ , showing excellent agreement. Fig. 5 shows a histogram of the difference between the eigenvalues of the denoiser and the approximation. We see that for small  $t = 0.1$  and small  $m = 2$  the approximation is very good, with the differences on the order of  $10^{-6}$ . For increasing  $t$  and  $m$  the eigenvalues start to deviate. With  $t$  it is clear that larger values lead to larger differences, when neglecting higher order terms in the BCH expansion. For  $m$  we note that increasing the number of layers leads to a larger number of higher order terms in the expansion.

Consequently, to understand the spectrum of the denoiser, we can focus on the sum of Lindbladians. Here we drop the tilde of the Lindbladians, as we are not comparing the exact denoiser to approximations, but making an observation about the ensemble of denoisers.

First we notice that the sum of Lindbladians  $\sum_i^m \mathcal{L}_i$  is still a Lindbladian:

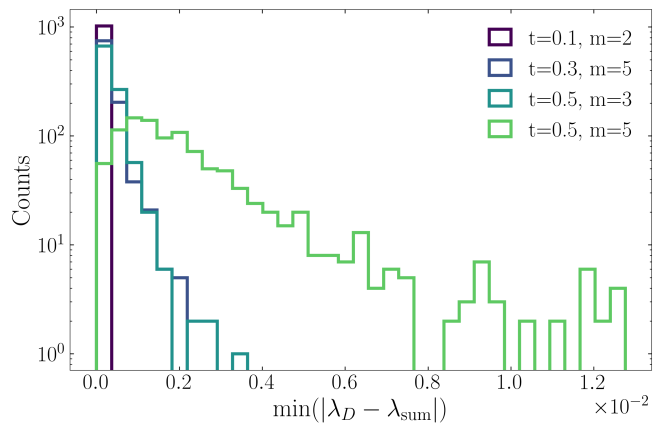


FIG. 5. Minimal distance between eigenvalues of the denoiser and the spectrum of  $\exp\left(-t \sum_i^m \tilde{\mathcal{L}}_i\right)$ , for  $N = 32$  and different combinations of  $t$  and  $m$ . For each eigenvalue we search for the minimal distance to an eigenvalue in the other spectrum. For  $t = 0.1, m = 2$  the largest deviation is at the order of  $10^{-6}$ . With  $t$  and  $m$  increasing the differences of the spectrum is also increasing.

$$\sum_{l,n=0}^{N^2-2} \sum_i^m (K_i)_{l,n} \left[ F_l \otimes F_n^* - \frac{1}{2} (F_n^\dagger F_l \otimes \mathbb{1} + \mathbb{1} \otimes F_l^T F_n^*) \right].$$

We thus expect to be able to predict the spectrum of the denoiser with the contour of the single Lindblad generator.

The center of the spectral support is given by the average of the eigenvalues of the Lindbladian, which is equivalent to the trace of the Lindblad generator divided by the dimension  $N^2$ . The trace of the Lindbladian is given by

$$\text{Tr} \mathcal{L} = -N \text{Tr}(K) = -N^2. \quad (16)$$

Since the trace is additive the trace of  $m$  Lindbladians is  $-mN^2$  and the average eigenvalue is  $\frac{\text{Tr}(\sum_i^m \mathcal{L}_i)}{N^2} = -m$ .

Finally, we have to understand the scaling of the support of a sum of Lindbladians in terms of the number of layers  $m$ . Here we draw on the results of [27, 28], which show that the expected spectral norm of a sum of independent random matrices scales as  $\sqrt{m}$ . This means that the extent of the spectrum of a sum of independent Lindblad generators scales as  $\sqrt{m}$ .

With this we can predict the contour of the denoiser spectrum to be similar to that of a single Lindbladian with the center of the support at  $-m$  and the extent scaling as  $\sqrt{m}$ .

Given points  $\{f_{\mathcal{L},i}\}, i \in \mathbb{N}$  on the contour of the Lindblad spectrum with center at 0 and extent  $2/N$ , as described in [15], the reasoning above shows that the contour of the denoiser spectrum can be approximated by a

map  $g$ , that connects the contour of the Lindblad spectrum to the contour of the denoiser spectrum:

$$f_{D,i} = g(f_{\mathcal{L},i}) = \exp(-t(\sqrt{m}f_{\mathcal{L},i} - m)). \quad (17)$$

We can compare this prediction  $\{f_{D,i}\}$  with the numerically calculated spectrum of the denoiser, shown in Fig. 6. We see that the spectrum of the denoiser is well described by the prediction and it holds for  $t < 1$ . In contrast to the comparison of the BCH expansion to the exact denoiser, this prediction holds for a larger parameter regime, as it only describes the lemon-like shape of the spectral support.

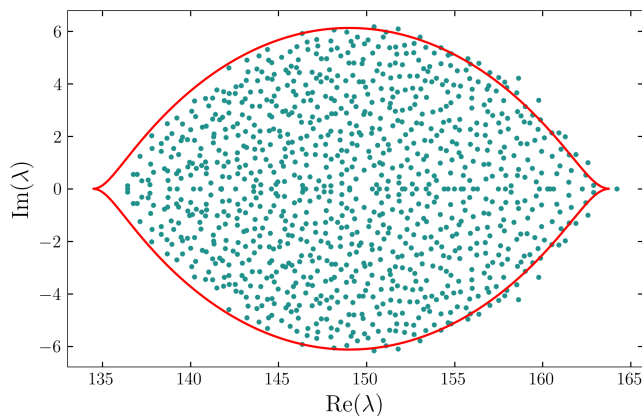


FIG. 6. Comparison of the denoiser spectrum and the boundary of its support in the complex plane predicted by Eq. 17 for  $N = 32$ ,  $t = 0.5$  and  $m = 10$ . We see that the denoiser spectrum is well described by the predicted contour, which is shown in red. For readability we exclude the steady state at 1.

The only deviation is to the side of larger modulus, where a few eigenvalues lie outside of the predicted contour. This is likely due to the finite size effects of the Lindblad spectrum. We show in appendix A, Fig. 10 the spectra of shifted and rescaled Lindblad generators for different  $N$ . We see that for smaller  $N$  the Lindblad spectrum has eigenvalues outside the contour with smaller modulus. A smaller modulus in the Lindblad spectrum translates to a larger modulus in the denoiser spectrum. For increased systemsize  $N$  the Lindblad spectrum condenses better into the predicted contour, which should lead to a better agreement of the denoiser spectrum with the prediction.

Additionally the map  $g$  implies that the middle of the denoiser spectrum lies at  $\exp(tm)$ , which we can confirm in Fig. 2.

## V. LOCAL NOISE

The full rank Lindbladian discussed above is an idealized model of the noise. In other works it was found that

the noise in current quantum hardware is best described by local noise channels [5, 29–31]. Because of this reason we want to impose a notion of locality on the noise.

To do so we use Pauli strings  $s_l = \sigma_{x_1} \otimes \sigma_{x_2} \otimes \dots \otimes \sigma_{x_L} / \sqrt{N}$  ( $x_i \in x, y, z, \mathbb{1}$ ) to form the operator basis  $F_l$  of the Lindblad generator. The number of non-identity Pauli matrices, also known as Pauli weight,  $k = \sum_i^L (1 - \delta_{x_i,1})$  in the string  $s_l$  denotes the locality of the operator. We say a Lindbladian is  $k_{\max}$ -local if all  $s_l$  with Pauli weight  $k < k_{\max}$  are included in the operator basis. Consequently, the Kossakowski matrix  $K$  has dimension  $N_L = \sum_{k_i}^{k_{\max}} \binom{L}{k_i} 3^{k_i}$ . We generate  $K$  from a diagonal matrix with positive entries, which is then rotated by a random unitary matrix, with respect to the Haar measure, on  $U(N_L)$ . This ensures that  $K$  is positive semi-definite.

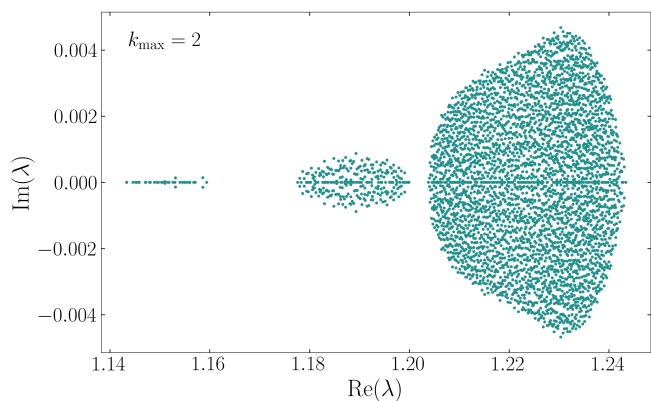


FIG. 7. Denoiser spectrum for local Lindblad generators, with  $N = 64$ ,  $t = 0.1$ ,  $m = 2$  and  $k_{\max} = 2$ . The spectrum shows multiple timescales of decay, which originate from the locality of the Lindbladian.

The local Lindbladian is then given as,

$$\mathcal{L}_L = \sum_{l,m=1}^{N_L} K_{m,l} \left[ s_l \otimes s_m^* - \frac{1}{2} (s_m^\dagger s_l \otimes \mathbb{1} + \mathbb{1} \otimes s_l^T s_m^*) \right].$$

This formulation is equivalent to the one used in [16], where it was found that the spectrum of these local Lindblad generators show multiple levels of decay depending on the locality  $k_{\max}$ . In appendix A Fig. 9 we show that we reproduce the spectra obtained in [16].

In order to have a fair comparison between the local noise case and the global case we normalize the Kossakowski matrix to  $N$ . This ensures that the average of the eigenvalues is still at  $-1$ .

The denoiser spectrum for Lindbladians with locality  $k_{\max} = 2$  is shown in Fig. 7 and we show the other localities in the appendix E, Fig. 12. We see that the denoiser spectrum shows multiple levels in its spectrum. This is a direct consequence of the multiple levels in the Lindblad spectrum, which are inherited by the denoiser in accordance with Eq. 15. In appendix C we show the comparison of the denoiser spectrum with the prediction

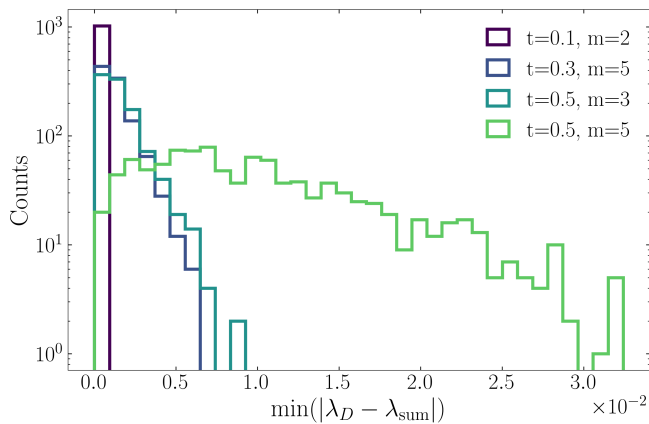


FIG. 8. Minimal distance between eigenvalues of the denoiser and the spectrum of  $\exp\left(-t\sum_i^m \tilde{\mathcal{L}}_{L_i}\right)$ , for  $N = 32$  and different combinations of  $t$  and  $m$ . For each eigenvalue we search for the minimal distance to an eigenvalue in the other spectrum. For  $t = 0.1, m = 2$  the largest deviation is at the order of  $10^{-4}$ . With  $t$  and  $m$  increasing the differences of the spectra is also increasing.

made in Eq. 15 in Fig. 11. Here we show the histogram of the difference between the approximation and the exact solution in Fig. 8. We see that the approximation is working well also in the local case.

## VI. CONCLUSION

We considered an ensemble of random noisy quantum circuits without structure and an accompanying denoising operator, which inverts the noise of the environment. In the case that the Lindbladian noise is global we showed that the spectrum of the denoiser in the complex plane can be predicted by the universal spectrum of a single random Lindblad generator first shown in [15].

In the case of few-qubit noise channels, which we consider more realistic for current hardware with few-qubit gates, the spectrum of the denoiser exhibits different decay rates inherited from the spectra of random few-body Liouvillians [16].

For a small noise parameter  $t$  and for small numbers of layers  $m$ , the denoiser can be expanded to first order in  $t$  as an exponential of the sum of the generating Lindbladians, transformed by the unitary layers of the circuit, allowing for an analytical connection between the spectra of random Liouvillians and denoisers to understand the origin of the spectral features.

While denoisers must correspond to unphysical processes and cannot even be defined for a non-invertible noise channels, our results reveal an unexpected feature: The locality structure of the underlying noise survives the scrambling of random circuits. This persistence of locality-induced spectral structure indicates that, in realistic settings, effective denoisers may be implementable by relatively shallow circuits built from few-body gates.

## VII. ACKNOWLEDGEMENTS

This project has received funding from the European Union’s Horizon 2020 research and innovation programme under Grant Agreement No. 101017733 and from the Deutsche Forschungsgemeinschaft (DFG) through the project DQUANT (project-id 499347025). We acknowledge support from the DFG through the Collaborative Research Centers CRC TR185 OSCAR (No. 277625399) and CRC 1639 NuMerIQS (project-id 511713970) as well as through the cluster of excellence ML4Q (EXC 2004, project-id 39053476).

KŻ acknowledges support by the European Union under ERC Advanced Grant Tatypic, Project No. 101142236.

The authors gratefully acknowledge the granted access to the Marvin cluster hosted by the University of Bonn.

- 
- [1] J. Preskill, Quantum computing in the NISQ era and beyond, *Quantum* **2**, 79 (2018).
  - [2] M. Dinca, D. J. Luitz, and M. Debertolis, *Quantum process tomography of a compressed time evolution circuit on superconducting quantum processors* (2025), 2509.25342.
  - [3] K. Temme, S. Bravyi, and J. M. Gambetta, Error mitigation for short-depth quantum circuits, *Physical Review Letters* **119**, 180509 (2017).
  - [4] R. S. Gupta, E. v. d. Berg, M. Takita, D. Riste, K. Temme, and A. Kandala, Probabilistic error cancellation for dynamic quantum circuits, *Phys. Rev. A* **109**, 062617 (2024).
  - [5] E. v. d. Berg, Z. K. Mineev, A. Kandala, and K. Temme, Probabilistic error cancellation with sparse Pauli-Lindblad models on noisy quantum processors, *Nature Physics* **19**, 1116 (2023).
  - [6] A. Kandala, K. Temme, A. D. Córcoles, A. Mezzacapo, J. M. Chow, and J. M. Gambetta, Error mitigation extends the computational reach of a noisy quantum processor, *Nature* **567**, 491–495 (2019).
  - [7] T. Scheiber, P. Haubenwallner, and M. Heller, Reduced sampling overhead for probabilistic error cancellation by Pauli error propagation, *Quantum* **9**, 1840 (2025).
  - [8] S. Ferracin, A. Hashim, J.-L. Ville, R. Naik, A. Carignan-Dugas, H. Qassim, A. Morvan, D. I. Santiago, I. Siddiqi, and J. J. Wallman, Efficiently improving the performance of noisy quantum computers, *Quantum* **8**, 1410 (2024).
  - [9] R. Takagi, S. Endo, S. Minagawa, and M. Gu, Fundamental limits of quantum error mitigation, *npj Quantum Information* **8**, 114 (2022).
  - [10] Y. Kim, A. Eddins, S. Anand, K. X. Wei, E. van den Berg, S. Rosenblatt, H. Nayfeh, Y. Wu, M. Zaletel, K. Temme, and A. Kandala, Evidence for the utility of

- quantum computing before fault tolerance, *Nature* **618**, 500 (2023).
- [11] D. Aharonov and M. Ben-Or, Fault-tolerant quantum computation with constant error rate, *SIAM Journal on Computing* **38**, 1207 (2008).
- [12] A. Y. Kitaev, Quantum computations: algorithms and error correction, *Russian Mathematical Surveys* **52**, 1191 (1997).
- [13] P. W. Shor, Scheme for reducing decoherence in quantum computer memory, *Physical Review A* **52**, R2493 (1995).
- [14] M. S. J. Tepaske and D. J. Luitz, Compressed quantum error mitigation, *Physical Review B* **107**, L201114 (2023).
- [15] S. Denisov, T. Lapyteva, W. Tarnowski, D. Chruściński, and K. Życzkowski, Universal spectra of random Lindblad operators, *Physical Review Letters* **123**, 140403 (2019).
- [16] K. Wang, F. Piazza, and D. J. Luitz, Hierarchy of relaxation timescales in local random Liouvillians, *Physical Review Letters* **124**, 100604 (2020).
- [17] L. Sá, P. Ribeiro, T. Can, and T. Prosen, Spectral transitions and universal steady states in random Kraus maps and circuits, *Physical Review B* **102**, 134310 (2020).
- [18] C. Timm, Random transition-rate matrices for the master equation, *Physical Review E* **80**, 021140 (2009).
- [19] S. Lange and C. Timm, Random-matrix theory for the Lindblad master equation, *Chaos: An Interdisciplinary Journal of Nonlinear Science* **31**, 023101 (2021).
- [20] O. E. Sommer, F. Piazza, and D. J. Luitz, Many-body hierarchy of dissipative timescales in a quantum computer, *Physical Review Research* **3**, 023190 (2021).
- [21] A. Kossakowski, On the general form of the generator of a dynamical semi-group for the spin 1/2 system, *Bull. Acad. Pol. Sci., Ser. Sci. Math. Astron. Phys.* **21**, 649 (1973).
- [22] G. Lindblad, On the generators of quantum dynamical semigroups, *Communications in Mathematical Physics* **48**, 119 (1976).
- [23] K. Życzkowski and H.-J. Sommers, Induced measures in the space of mixed quantum states, *Journal of Physics A: Mathematical and General* **34**, 7111–7125 (2001).
- [24] M. Fasi and L. Robol, Sampling the eigenvalues of random orthogonal and unitary matrices, *Linear Algebra and its Applications* **620**, 297 (2021).
- [25] F. Mezzadri, How to generate random matrices from the classical compact groups (2007), [math-ph/0609050](https://arxiv.org/abs/math-ph/0609050).
- [26] M.-D. Choi, Completely positive linear maps on complex matrices, *Linear Algebra and its Applications* **10**, 285 (1975).
- [27] J. A. Tropp, The expected norm of a sum of independent random matrices: An elementary approach, in *High Dimensional Probability VII*, edited by C. Houdré, D. M. Mason, P. Reynaud-Bouret, and J. Rosiński (Springer International Publishing, Cham, 2016) pp. 173–202.
- [28] L. Sá, P. Ribeiro, and T. Prosen, Spectral and steady-state properties of random liouvillians, *Journal of Physics A: Mathematical and Theoretical* **53**, 305303 (2020).
- [29] S. Mangini, M. Cattaneo, D. Cavalcanti, S. Filippov, M. A. C. Rossi, and G. García-Pérez, Tensor network noise characterization for near-term quantum computers, *Phys. Rev. Res.* **6**, 033217 (2024).
- [30] D. Brand, I. Sinayskiy, and F. Petruccione, Markovian noise modelling and parameter extraction framework for quantum devices, *Scientific Reports* **14**, 4769 (2024).
- [31] G. Di Bartolomeo, M. Vischi, F. Cesa, R. Wixinger, M. Grossi, S. Donadi, and A. Bassi, Noisy gates for simulating quantum computers, *Phys. Rev. Res.* **5**, 043210 (2023).
- [32] R. Speicher, *Free probability and random matrices* (2014), [arXiv:1404.3393](https://arxiv.org/abs/1404.3393).
- [33] M. A. Nowak and W. Tarnowski, Spectra of large time-lagged correlation matrices from random matrix theory, *Journal of Statistical Mechanics: Theory and Experiment* **2017**, 063405 (2017).
- [34] D. V. Voiculescu, K. J. Dykema, and A. Nica, *Free random variables*, Vol. 1 (American Mathematical Society, Providence, RI, 1992).
- [35] J.-P. Lund, R. S. Strichartz, and J. P. Vinson, Cauchy transforms of self-similar measures, *Experimental Mathematics* **7**, 177 (1998).

### A. APPENDIX A: SPECTRA OF LINDBLADIANS

Here we show the spectra of the Lindblad generators used in the main text.

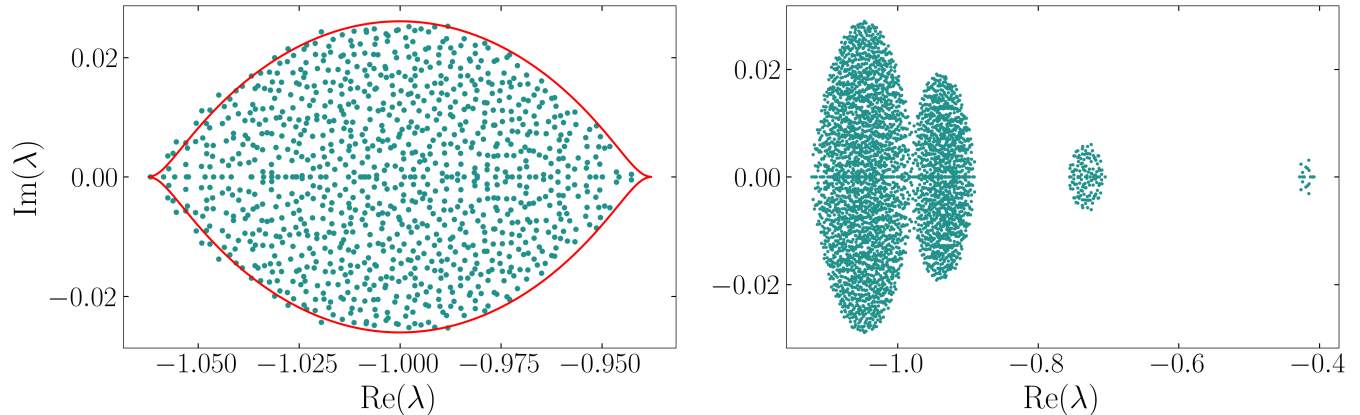


FIG. 9. Left: Spectra of Lindbladians, for  $N = 32$ . The spectra are resembling the universal behavior with the support bounded to the subset of the complex plane described in [15] and represented by a red curve. Right: Spectra of local Lindbladians, for  $N = 64$  and  $k_{\max} = 2$ . We see multiple distinguishable decay rates and it reproduces the spectra found in [16].

In Fig. 10 we show the spectra of global Lindblad generators for different system sizes. For smaller system sizes we see deviations from the random matrix theory. Since the spectra agree better for larger system sizes we conclude that this is due to the finite size effect.

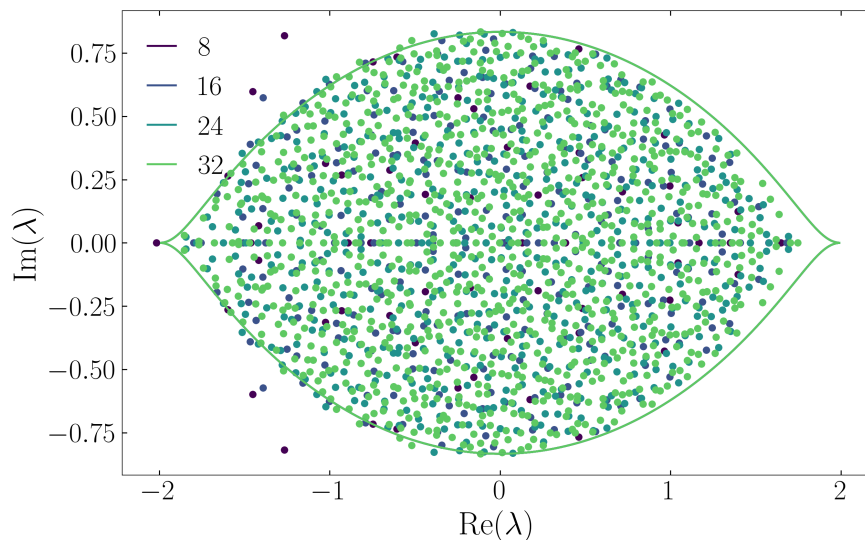


FIG. 10. Rescaled and shifted spectra of Lindbladians, for different system sizes  $N = [8, 16, 24, 32]$ . We see that for larger system sizes the lemon-like shape derived in [15] and the spectra agree better, indicating a finite size effect.

### B. APPENDIX B: TRACE OF LINDBLADIANS

Here we show the short calculation of the trace of a Lindblad generator.

$$\begin{aligned}
\text{Tr} \mathcal{L} &= \text{Tr} \left( \sum_{l,p=0}^{N^2-2} K_{p,l} \left[ F_l \otimes F_p^* - \frac{1}{2} (F_p^\dagger F_l \otimes \mathbb{1} + \mathbb{1} \otimes F_l^T F_p^*) \right] \right) \\
&= \sum_{l,p=0}^{N^2-2} K_{p,l} \left[ \text{Tr}(F_l) \text{Tr}(F_p^*) - \frac{1}{2} (\text{Tr}(F_p^\dagger F_l) \text{Tr}(\mathbb{1}) + \text{Tr}(\mathbb{1}) \text{Tr}(F_l^T F_p^*)) \right] \\
&= \sum_{l,p=0}^{N^2-2} K_{p,l} \left[ 0 - \frac{1}{2} (\delta_{p,l} N + N \delta_{p,l}) \right] \\
&= -N \text{Tr}(K) \\
&= -N^2,
\end{aligned}$$

where we used that  $\text{Tr}(\mathbb{1}) = N$ ,  $\text{Tr}(F_i^\dagger F_j) = \delta_{ij}$  and that the  $F_l$  are traceless. The trace of the Kossakowski matrix is chosen to be  $N$ , so that the trace of the sum of Lindbladians is

$$\text{Tr} \left( \sum_i^m \mathcal{L}_i \right) = -N \text{Tr} \left( \sum_i^m K_i \right) = -N^2 m.$$

Since the dimension of the Lindblad generator is  $N^2$  the center of the spectral support is at  $\frac{\text{Tr}(\sum_i^m \mathcal{L}_i)}{N^2} = -m$ .

### C. APPENDIX C: APPROXIMATING DENOISER AS SUM OF LINDBLADIANS

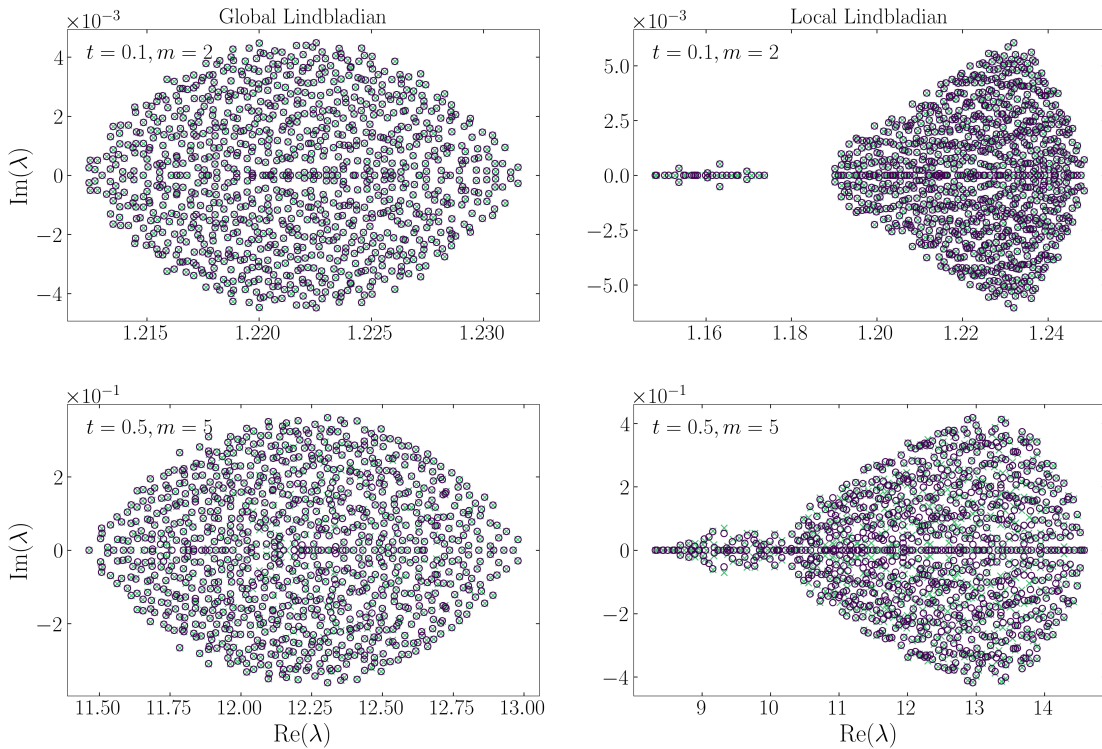


FIG. 11. Comparison of the denoiser spectrum (x) and the spectrum of  $\exp\left(-t \sum_i^m \tilde{\mathcal{L}}_i\right)$  (o) in the complex plane; for  $N = 32$ ,  $t = 0.1, m = 2$  and  $t = 0.5, m = 5$ , for global Lindbladians (left) and local Lindbladian  $k_{\max=2}$  (right). The spectra agree well, showing that the sum of Lindbladians is a good approximation of the denoiser for this parameter regime. For larger  $t$  and  $m$  the eigenvalues start to deviate. For readability we exclude the stationary point at 1.

The spectra of the exact denoiser and the approximations by the sum of Lindblad generators (eq 15) are shown in Fig. 11 for the global and local case. We can see that the spectra agree well in both cases, showing that the sum of Lindbladians is a good approximation of the denoiser for this parameter regime. It was found that the commutators of random Lindblad generators are small. This explains why the linear approximation is good, even for larger  $t$ . This approximation was found to be most sensitive to the number of layers  $m$ .

#### D. APPENDIX D: SUM OF KOSSAKOWSKI MATRICES

The denoiser operator is inherently linked to a sum of Lindblad generators, as it is the leading term in the BCH expansion. To understand the spectrum of the denoiser, we should understand the spectrum of the sum of Lindbladians. A sum of Lindbladians can be reduced to a sum of  $m$  Kossakowski matrices,

$$\sum_i^m \mathcal{L}_i = \sum_{l,n=0}^{N^2-2} \left( \sum_i^m K_i \right)_{l,n} [F_l \otimes F_n^* - \frac{1}{2}(F_n^\dagger F_l \otimes 1 + 1 \otimes (F_n^\dagger F_l)^T)],$$

where the  $K$  are sampled as explained in the main text. The idea is then that the spectrum of the sum of Lindbladians is related to the spectrum of the sum of Kossakowski matrices. We are interested in the scaling of the spectrum with the number of layers  $m$ . The spectra of the Kossakowski matrices are real, positive and follow the Marchenko-Pastur distribution. We can use the framework of free probability theory [32–34] to calculate the spectrum of the sum of these random matrices. This framework was used in [15] to calculate the spectrum of the Lindblad operators. We can use the same framework to calculate the bounds of the spectrum of the sum of Kossakowski matrices. Since the eigenvalues of the Kossakowski matrices are real and positive, we can use the R-transform to calculate the spectrum. The R-transform of the sum of Kossakowski matrices is given by

$$R(z) = \frac{1}{1-z},$$

where  $z$  is a complex number. The R-transform of the sum of Kossakowski matrices is in turn given by the sum of the R-transforms of the individual Kossakowski matrices

$$R(z) = \frac{m}{1-z}.$$

The spectrum of the sum of Kossakowski matrices can be calculated from the Cauchy transform  $G(z)$ , which is related to the R-transform [32, 35] by

$$R(G(z)) + \frac{1}{G(z)} = z.$$

With the explicit form of the R-transform we can calculate the Cauchy transform

$$\begin{aligned} \frac{m}{1-G(z)} + \frac{1}{G(z)} &= z, \\ mG(z) + 1 - G(z) &= zG(z) - zG(z)^2, \\ zG(z)^2 - G(z)(m-1-z) + 1 &= 0. \end{aligned}$$

The solution of this quadratic equation is given by

$$G(z) = \frac{(z-m+1) \pm \sqrt{(m-1-z)^2 - 4z}}{2z}.$$

The spectrum is then given as

$$\rho(z) = \frac{1}{\pi} \lim_{\epsilon \rightarrow 0^+} \text{Im}[G(z+i\epsilon)].$$

Since the eigenvalues of the sum  $z$  are purely real we can ignore the first term and focus on the square root. The square root is imaginary if the contents are negative. Thus we can search for the roots of  $\frac{(m-1-z)^2}{4z^2} - \frac{1}{z}$ :

$$\begin{aligned} \frac{(m-1-z)^2}{4z^2} - \frac{1}{z} &= 0, \\ (m-1-z)^2 - 4z &= 0, \\ z^2 - z(2(m-1)+4) + (m-1)^2 &= 0. \end{aligned}$$

The solutions are then the boundaries of the spectrum we are looking for:

$$z = m + 1 \pm \sqrt{(m + 1)^2 - (m - 1)^2},$$

$$z = m + 1 \pm 2\sqrt{m}.$$

We find that the scaling of the boundaries of the spectrum is proportional to  $\sqrt{m}$ , which is the same scaling found for the sum of Lindbladians.

### E. APPENDIX E: DENOISER SPECTRA FOR DIFFERENT LOCALITIES $k_{\max}$

Here we show the denoiser spectra for different localities  $k_{\max}$  in the Lindblad generators. The spectra feature the characteristic clustering known from previous work on random local Lindblad generators [16] depending on the locality  $k_{\max}$ .

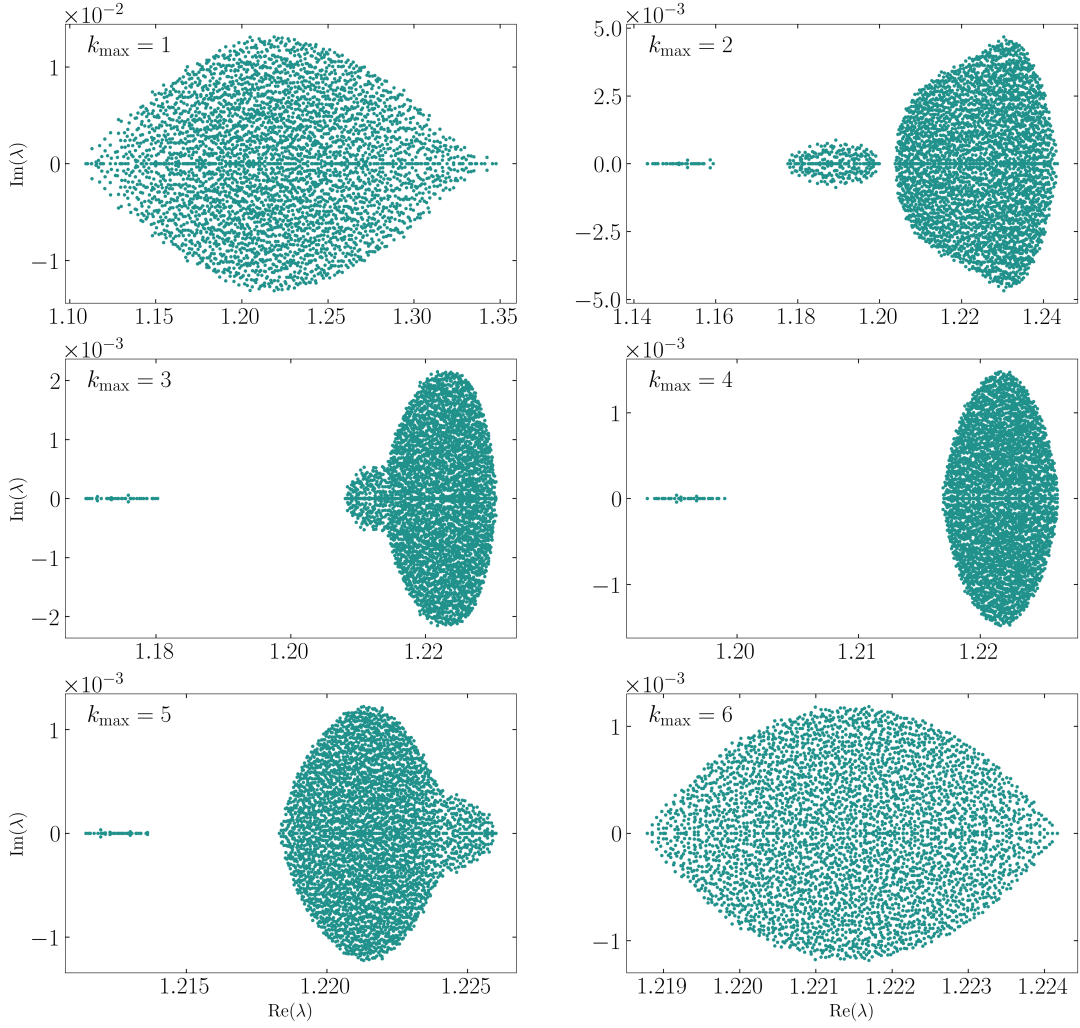


FIG. 12. Denoiser spectra for different localities  $k_{\max}$  of the Lindbladians, with  $N = 64 = 2^6$ ,  $t = 0.1$  and  $m = 2$ . The spectrum shows multiple levels of decay, which are related to the locality of the Lindbladian. For  $k_{\max} = L$  the denoiser spectrum reproduces the one of global Lindbladians shown in Fig. 4.